

Driving in Corner Case: A Real-World Adversarial Closed-Loop Evaluation Platform for End-to-End Autonomous Driving

Jiaheng Geng¹, Jiatong Du¹, Xinyu Zhang¹, Ye Li¹, Panqu Wang², Yanjun Huang¹✉

Abstract—Safety-critical corner cases, difficult to collect in the real world, are crucial for evaluating end-to-end autonomous driving. Adversarial interaction is an effective method to generate such safety-critical corner cases. While existing adversarial evaluation methods are built for models operating in simplified simulation environments, adversarial evaluation for real-world end-to-end autonomous driving has been little explored. To address this challenge, we propose a closed-loop evaluation platform for end-to-end autonomous driving, which can generate adversarial interactions in real-world scenes. In our platform, the real-world image generator cooperates with an adversarial traffic policy to evaluate various end-to-end models trained on real-world data. The generator, based on flow matching, efficiently and stably generates real-world images according to the traffic environment information. The efficient adversarial surrounding vehicle policy is designed to model challenging interactions and create corner cases that current autonomous driving systems struggle to handle. Experimental results demonstrate that the platform can generate realistic driving images efficiently. Through evaluating the end-to-end models such as UniAD and VAD, we demonstrate that based on the adversarial policy, our platform evaluates the performance degradation of the tested model in corner cases. This result indicates that this platform can effectively detect the model’s potential issues, which will facilitate the safety and robustness of end-to-end autonomous driving.

I. INTRODUCTION

End-to-end autonomous driving has attracted significant attention in both academia and industry. By directly mapping inputs such as images to driving actions within a unified framework [1], [2], this paradigm simplifies the system while enhancing generalization [3]–[5]. End-to-end autonomous driving has become one of the most active research directions in autonomous driving.

For autonomous driving, safety-critical corner cases can identify the boundary of model capability and are important for model evaluation. However, corner cases are difficult to collect in the real world [6], [7]. Many studies have shown that developing adversarial policies for surrounding vehicles can efficiently generate safety-critical corner cases [8]–[10]. Existing autonomous driving simulators can control traffic flows to generate adversarial scenarios [11]–[13]. But the corner cases created by these simulators suffer from a significant sim-to-real gap in visual realism: the model trained on real-world datasets cannot be evaluated. Therefore, it is imperative to establish an adversarial closed-loop evaluation platform for real-world scenes.

To address the sim-to-real gap in visual realism, many researchers employ driving image generation methods. Some studies employ world models to predict future real-world scenes [14]–[16], where historical latent information is propagated to estimate future states and decode them into future images. However, such methods often suffer from weak controllability over the generated images, while adversarial scenarios require strong controllability over surrounding vehicles, which is clearly contradictory. Diffusion-based approaches for driving dataset generation enable conditional controllability [17]–[20]. Challenger [21] creates conditions that induce adversarial scenarios, thereby generating adversarial nuScenes-like datasets. Nevertheless, it still lacks closed-loop evaluation, as the ego has no interactivity. DriveArena [22] integrates SUMO with an image generation model to achieve closed-loop simulation, but the surrounding vehicles are not adversarial. As a result, the discovery of corner cases remains inefficient, and the testing routes are cluttered with redundant and stable traffic conditions. In summary, current methods lack adversarial interactions and cannot create effective corner cases for end-to-end autonomous driving closed-loop evaluation.

Many researchers generate corner cases by manipulating surrounding vehicles to interact adversarially with the ego. A common approach is to employ reinforcement learning (RL) to enable surrounding vehicles to learn policies that challenge the ego [23]–[26]. Wang et al. [25] leverage RL combined with dynamic and static scene exploration to rapidly search for adversarial safety-critical cases. L2C [26] integrates generative models with RL to efficiently generate such scenarios. Moreover, methods like KING [6] and STRIVE [7] adopt trajectory optimization through cost-function backpropagation, endowing basic trajectory prediction algorithms with adversarial capabilities. However, RL-based approaches are often constrained by their training scenes, limiting their application, and gradient backpropagation is computationally expensive and inefficient [27]. These impose a heavy burden on efficient closed-loop evaluation with real-world image generation. Recently, multimodal trajectory prediction methods have offered new directions for adversarial policy [27], [28]. In this work, by filtering trajectories based on their adversarial scores, the surrounding vehicle can efficiently get the adversarial policy.

For closed-loop simulation in real-world scenarios, efficiency is of paramount importance. Reducing the number of denoising steps is a key approach to accelerating image generation for diffusion models [29]–[31], but the generation process still requires tens to hundreds of denoising steps [32].

¹School of Automotive Studies, Tongji University, Shanghai, China.

²ZERON, Jiangsu, China.

✉ Corresponding author

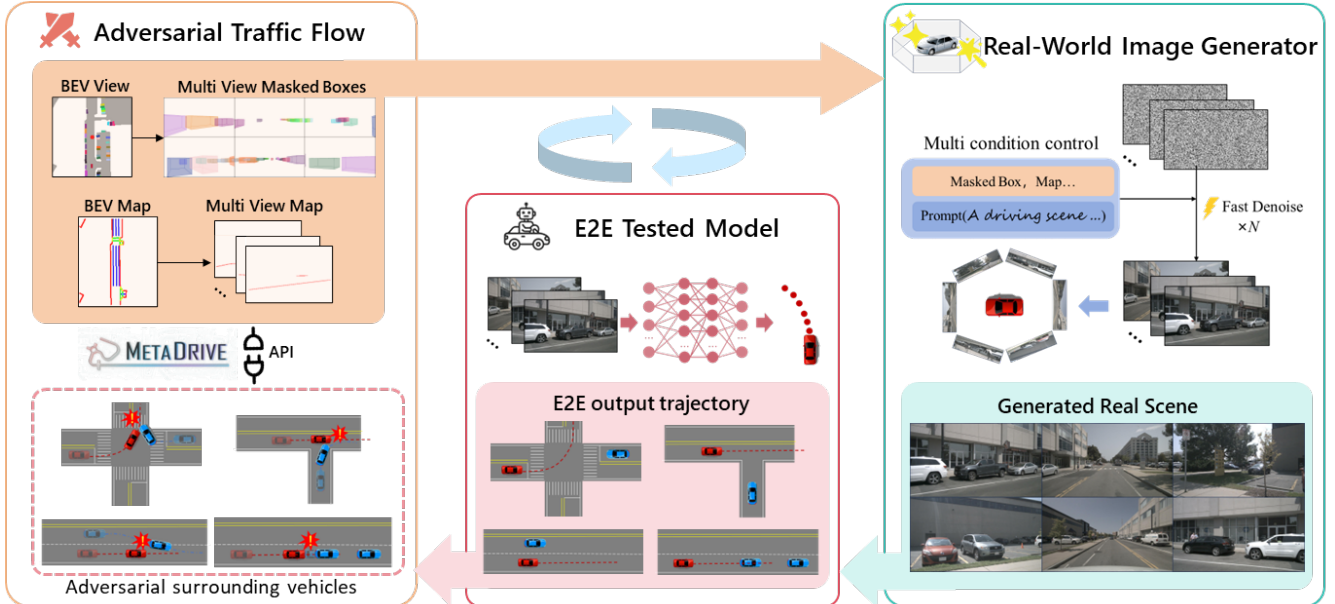


Fig. 1: **Overview of the real-world adversarial closed-loop evaluation platform.** The platform integrates three key modules: Adversarial Traffic Flow, Real-World Image Generator, and E2E Tested Model. The Adversarial Traffic Flow generates surrounding vehicles that interact adversarially with the ego, providing traffic information to the Real-World Image Generator. The generator efficiently generates real-world images based on traffic information through flow matching. The generated images are passed as input to the E2E Tested Model, and the model’s output is fed back to the Adversarial Traffic Flow, completing the closed-loop simulation.

Reducing steps often degrades the quality of generation [33], thereby undermining the realism of the simulation. Flow matching [34] offers a promising solution to this trade-off. By reformulating the stochastic differential equation (SDE) of the diffusion process into a deterministic ordinary differential equation (ODE) [29], it enables high-quality image generation under a few denoising steps, thus significantly improving both the efficiency and the realism of closed-loop simulation in real-world scenarios.

This work proposes a real-world adversarial closed-loop evaluation platform for end-to-end autonomous driving, in which the real-world image generator collaborates with an adversarial traffic policy to evaluate end-to-end models in corner cases. Specifically, the generator correspondingly generates real-world images according to traffic conditions, such as lane markings and the distribution of surrounding objects. The flow matching-based model in the generator ensures efficiency and realism. Moreover, by filtering the trajectories of multi-modal outputs to find the adversarial and reasonable ones, surrounding vehicles can efficiently follow adversarial policies. The experiment shows that generated images with low denoising steps in this platform outperform the baseline in terms of realism metrics. Our platform supports evaluating various end-to-end model instances. The results show that the adversarial traffic flow results in a sharp reduction of their scores and completion rates, effectively uncovering real-world corner cases that are difficult for the tested models to handle. Based on this design, the main contributions of this work are summarized as follows:

- 1) We introduce the first closed-loop evaluating platform with real-world adversarial scenarios, which can evaluate the performance of various end-to-end models under adversarial interactions.
- 2) The real-world image generator based on the traffic condition accordingly generates the real-world scene, in which the flow matching-based model using diffusion model priors can create high-quality real-world images with only a few denoising steps.
- 3) The adversarial traffic flow can quickly create adversarial scenarios according to the adversarial scores of surrounding vehicles’ multimodal trajectories. This adversarial policy is applicable to various tested models and traffic scenarios.

II. METHODOLOGY

This section presents the proposed closed-loop platform with real-world adversarial scenarios. First, provide an overview of the platform, describing its operation and the information flow. Then, introduce the adversarial policy of surrounding vehicles, followed by the flow matching-based generator. Finally, present the evaluation metrics.

A. Overall Architecture

As illustrated in Fig. 1, the proposed platform establishes a closed loop among three modules: Adversarial Traffic Flow, Real-World Image Generator, and the E2E Tested Model. The Adversarial Traffic Flow is driven by an autonomous driving simulator to provide a realistic vehicle

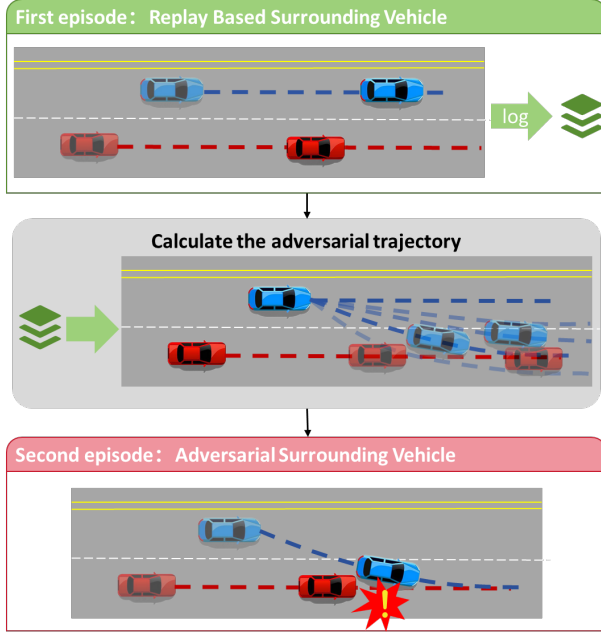


Fig. 2: **Adversarial surrounding vehicle generation method.** The method consists of two episodes. The first episode replays a steady traffic flow, and the trajectory of the tested model is recorded. Based on the recorded data, an adversarial and physically plausible trajectory of the surrounding vehicle is selected, and then this trajectory is applied in the second episode.

physical simulation. In this work, we adopt the lightweight MetaDrive [12] as the basis for Adversarial Traffic Flow, leveraging its rich interfaces for environment and traffic participant information to obtain traffic conditions such as maps and surrounding vehicle distributions. This information is then passed to the Real-World Image Generator. The flow matching-based generator generates real-world scene images conditioned on the ego's current traffic information, while ensuring compatibility with the input format of the end-to-end tested model. The E2E Tested Model takes the generated images as input and outputs the planned trajectory of the ego, which is subsequently fed back to the Adversarial Traffic Flow. The traffic flow then executes the ego's trajectory, thereby completing the closed-loop evaluation of real-world adversarial scenarios.

B. Adversarial Traffic Flow

Adversarial Traffic Flow is responsible for loading various traffic scenarios and evaluation process management. This section mainly introduces the structure and adversarial traffic policy.

1) *Two Episodes Architecture:* Due to different end-to-end models having various preferences, we adopt a two-episode architecture to ensure applicability across tested models, as illustrated in Fig. 2. Specifically, our platform adopts an epoch-based design, and one epoch consists of two episodes, where both episodes load the same real traffic

slice. The closed-loop shown in Fig. 1 is executed across both episodes. In the first episode, all surrounding vehicles replay the log, while the ego is controlled by the tested end-to-end model, and the complete trajectory of the ego is recorded. Before the second episode, the adversarial vehicle queries a multimodal trajectory prediction model and gets multiple candidate trajectories. Based on the ego trajectory recorded in the first episode, it selects the trajectory with the highest adversarial score and executes it in the second episode. In this way, the trajectory of the adversarial surrounding vehicle can be adjusted according to the trajectory preferences of different tested models

2) *Adversarial Score:* To generate surrounding vehicle trajectories that are both adversarial and physically plausible, we propose a multiplicative scoring function that jointly accounts for three key factors: (i) plausibility under the predictive model, (ii) likelihood of collision with the ego trajectory, and (iii) smoothness of motion. For each candidate trajectory τ_i , the scoring function is defined as:

$$\text{Score}(\tau_i) = p_i \cdot (c_i)^{w_c} \cdot e^{-w_j J(\tau_i)} \quad (1)$$

$$c_i = \gamma^{t_c(\tau_i)-1}$$

Where p_i denotes the prior probability output by the multimodal trajectory prediction model, ensuring that the generated adversarial trajectories remain consistent with realistic driving distributions; $c_i \in [0, 1]$ represents the collision possibility with the ego, designed such that earlier collisions yield higher values of c_i ; t_c is the first collision time step of τ_i , and $\gamma \in (0, 1)$ is the decay factor, together ensuring that trajectories leading to earlier collisions are prioritized during selection; $J(\tau_i)$ denotes the normalized jerk penalty, which discourages abrupt acceleration changes and enforces physical plausibility; and w_c and w_j are weighting parameters balancing the relative importance of adversarial intensity and motion smoothness. The final adversarial trajectory is defined as:

$$\tau^* = \arg \max_i \text{Score}(\tau_i) \quad (2)$$

With this design, the selected trajectory not only interacts with the ego adversarially but also avoids unrealistic or unstable motion patterns.

C. Real-World Image Generator

Diffusion models have demonstrated outstanding performance in generation tasks, particularly the foundation model of Stable Diffusion [35]. Although methods such as DDIM [36] attempt to reduce denoising steps, fewer denoising steps are often accompanied by lower quality. To address this, we adopt the ODE-based flow matching approach, employing the more computationally efficient Euler method for fast denoising and high image quality.

1) *Flow Matching:* Existing flow-matching models often require large parameter counts. In contrast, Stable Diffusion offers an efficient architecture and a rich ecosystem. Inspired by [37], we adopt a linear interpolation approach to transfer diffusion priors into flow-matching models, as shown at the

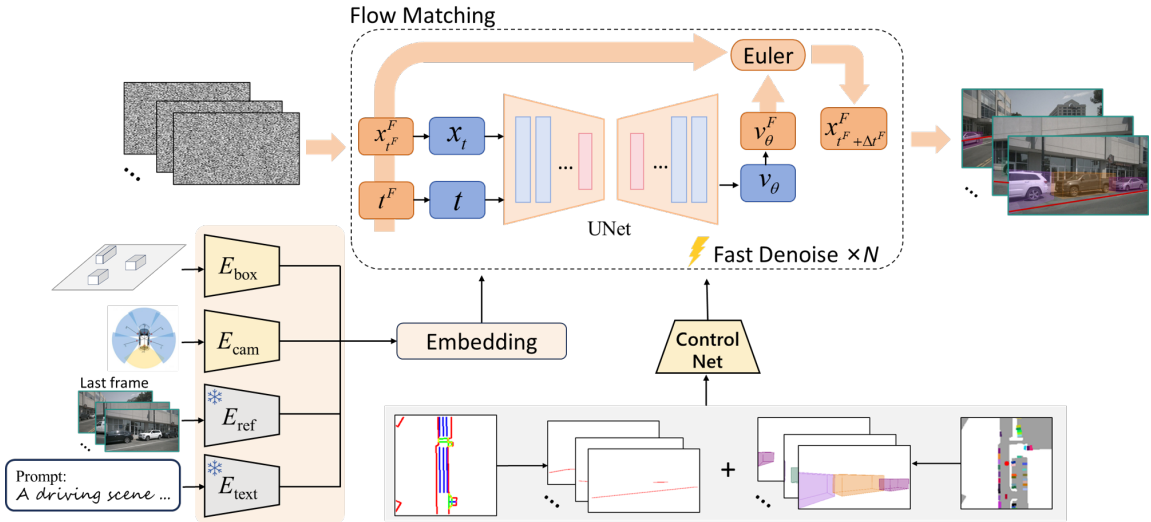


Fig. 3: **Overview of the Real-World Image Generator.** The backbone network of flow matching is a UNet, which leverages diffusion priors through linear transformation. Information projected into the camera view is injected via ControlNet, while other conditional information is incorporated through attention mechanisms.

top of Fig. 3, thereby combining pretrained priors with the efficient inference of flow matching.

The outputs of diffusion models generally take three common forms: noise, x_0 , and v_θ , which are equivalent. In our analysis, we adopt the v_θ . The noise-adding equation of the diffusion model and the parameterization of v_θ are defined in Eq. 3, t is the diffusion timestep.

$$\begin{bmatrix} x_t \\ v_\theta \end{bmatrix} = \begin{bmatrix} \alpha_t & \sigma_t \\ -\sigma_t & \alpha_t \end{bmatrix} \begin{bmatrix} x_0 \\ x_T \end{bmatrix}. \quad (3)$$

In diffusion model, α_t and σ_t satisfy $\alpha_t^2 + \sigma_t^2 = 1$, which allows us to inversely derive \hat{x}_0 and \hat{x}_T . The noise-adding equation and velocity v_θ^F definition in flow matching and conversion relationship are given in Eq. 4, t^F is the flow matching timestep. It should be noted that, following the conventions in diffusion and flow matching, x_0 and x_1^F denote the original data samples, whereas x_T and x_0^F represent random Gaussian noise.

$$\begin{cases} x_{t^F}^F = t^F x_1^F + (1 - t^F) x_0^F \\ v_\theta^F = x_1^F - x_0^F = \hat{x}_0 - \hat{x}_T \\ \quad = (\alpha_t - \sigma_t) x_t - (\alpha_t + \sigma_t) v_\theta \end{cases} \quad (4)$$

This conversion originates from linear algebra matrix inversion, which avoids retraining a nonlinear mapping from v_θ to the flow matching velocity v_θ^F through the network. This significantly reduces the training complexity while fully leveraging the prior knowledge embedded in the pretrained model. Moreover, t^F is defined as a continuous time in $[0, 1]$, whereas diffusion t usually adopt discrete steps (e.g., 0–999). The model still receives (t, x_t) , thus requiring a linear interpolation scheme to map between $x_{t^F}^F, t^F$ and t, x_t . Based on the noise-adding equation in Eq. 3 and Eq.

4, the conversion can be constructed shown in Eq. 5, and Eq. 6 demonstrates the Euler-based denoising. For the loss function, we use the mean squared error (MSE) between the v_θ^F and the $x_1^F - x_0^F$, as shown in Eq. 7.

$$\begin{cases} t^F = \alpha_t / (\alpha_t + \sigma_t) \in [0, 1] \\ x_{t^F}^F = t^F \cdot x_1 + (1 - t^F) \cdot x_0 = x_t / (\alpha_t + \sigma_t) \end{cases} \quad (5)$$

$$x_{t^F + \Delta t^F}^F = x_{t^F}^F + \Delta t^F \cdot v_\theta^F \quad (6)$$

$$\mathcal{L} = MSE((x_1^F - x_0^F), v_\theta^F) \quad (7)$$

2) *Condition Control*: To enable controllability over critical traffic elements in the generated images, we project the 3D bounding boxes of surrounding objects onto each camera view. To ensure consistency across viewpoints, each object is assigned a unique ID. When projecting the same object onto different views, the corresponding projection regions are masked according to this ID. A similar approach is applied to project lane markings into the various camera views. To maintain temporal consistency, we follow the approach in [22] by using the last frame as a reference, which provides better control over weather and street scenes. Additional auxiliary conditions include low-dimensional information such as camera intrinsic and extrinsic parameters and the coordinates of the 3D bounding boxes of surrounding objects.

We incorporate conditions through ControlNet and attention mechanisms, as illustrated in Fig. 3. The features of the reference image, prompts, and low-dimensional information are injected into the UNet through cross-attention. Based on the prompts of various times and weather, the generator can produce real-world images in different styles. Map and surrounding objects projected into the camera views are injected into the UNet using a trainable ControlNet.

	FID \downarrow				LPIPS \downarrow				SPI \downarrow			
	20 steps	10 steps	5 steps	3 steps	20 steps	10 steps	5 steps	3 steps	20 steps	10 steps	5 steps	3 steps
MagicDrive [20]	13.37	14.32	18.49	36.59	0.433	0.432	0.439	0.460	2.38	1.48	1.02	0.83
DriveArena [22]	14.17	15.65	20.00	32.99	0.354	0.353	0.359	0.382	2.44	1.53	1.06	0.85
Ours	12.05	12.92	15.64	23.63	0.323	0.319	0.320	0.338	2.43	1.52	1.04	0.85

TABLE I: **Comparison of the FID, LPIPS, and SPI.** The flow matching demonstrates an advantage in image quality under a few denoising steps, without increasing computational cost.

D. Evaluation Metrics

Our platform will quantitatively score the performance of the tested model under adversarial traffic flow. In the evaluation of autonomous driving, common single-frame metrics include no collisions (NC), drivable area compliance (DAC), ego progress (EP), time-to-collision (TTC), and comfort (C). Since we adopt real-world traffic slices, the ground-truth ego trajectory can be used as a reference, and the route completion (RC) can be derived. We also record the termination reason of each episode and determine whether the ego collides with surrounding vehicles, so the slice completion (SC) can be calculated after running all slices.

$$\text{PDMS} = \left(\underbrace{\prod_{m \in \{\text{NC}, \text{DAC}\}} \text{score}_m}_{\text{penalties}} \right) \times \left(\frac{\sum_{w \in \{\text{EP}, \text{TTC}, \text{C}\}} \text{weight}_w \times \text{score}_w}{\sum_{w \in \{\text{EP}, \text{TTC}, \text{C}\}} \text{weight}_w} \right) \quad (8)$$

The single-frame metrics indicate different aspects of driving performance. NAVSIM [38] proposed the PDMS by integrating these metrics, which has been widely adopted in both academia and industry, as shown in Eq. 8. Following this definition, we compute the average PDMS across the entire slice. The final closed-loop driving score (DS) is obtained by multiplying the average PDMS by the RC.

III. EXPERIMENTS

This section introduces the setups of the experiments, the realism of the images generated by Real-World Image Generator, and the experimental results of different tested end-to-end models on our platform.

A. Experimental Setups

1) *Real-World Image Generator*: We train and evaluate the image generator on the nuScenes dataset, and adopt Stable Diffusion 1.5 with a UNet–ControlNet architecture. For condition control, except for pretrained and frozen CLIP [39] for prompt and reference image encoders, other components are initialized and trained. Our baselines are DDIM-based image generation models, MagicDrive [20] and DriveArena [22], both built upon Stable Diffusion 1.5, which represent

the state-of-the-art controllable autonomous driving image generation methods.

Fast diffusion models based on DDIM typically adopt 50–100 denoising steps, while our image generator can achieve high image quality with a few denoising steps. We employ a fast denoising scheme with 10 steps and set the condition guidance scale to 2.0. For training, we use 8 NVIDIA A800 GPUs with an initial learning rate of 8×10^{-5} , which is gradually decayed during training. The batch size is set to 4, and the model is trained for 40 epochs.

2) *Closed-loop Setups*: We employ real driving slices from the Waymo Open Motion Dataset [40] and convert it into the format of MetaDrive for replay, where a diverse collection of traffic scene segments is gathered. The adversarial vehicle adopts the DenseTNT [41] multimodal trajectory prediction model, which outputs 32 candidate trajectories with prior probabilities. For the tested end-to-end models, we choose UniAD and VAD, both representative approaches in end-to-end autonomous driving. The closed-loop runs at 2Hz, while Adversarial Traffic Flow runs at 10Hz.

B. Image Generation Validation

To quantitatively evaluate the visual quality of the generated images, we adopt two common metrics: Fréchet Inception Distance (FID) and Learned Perceptual Image Patch Similarity (LPIPS). Specifically, FID measures the distributional discrepancy between generated and real images in the feature space, where lower values indicate higher fidelity; LPIPS evaluates perceptual similarity by comparing deep feature representations, thereby providing an assessment consistent with human perception. We conduct comparative experiments using the official pretrained weights of MagicDrive and DriveArena. To further validate the superiority of our generator under low denoising steps, we additionally report results with both low-step (5 and 3) and high-step (20) denoising settings. Moreover, the seconds per item (SPI) is recorded, i.e., the time required for a complete denoising process under the same computational resources. As summarized in TABLE I, our results demonstrate that under low denoising steps, both FID and LPIPS outperform the baselines without incurring additional runtime, confirming that the improvements are not achieved by scaling up the model or consuming extra resources. Considering efficiency and image quality, we select 10 steps for subsequent experiments.

To validate the effectiveness of key elements such as vehicles and lane markings in the generated images, we also use the validation set labels from nuScenes to generate

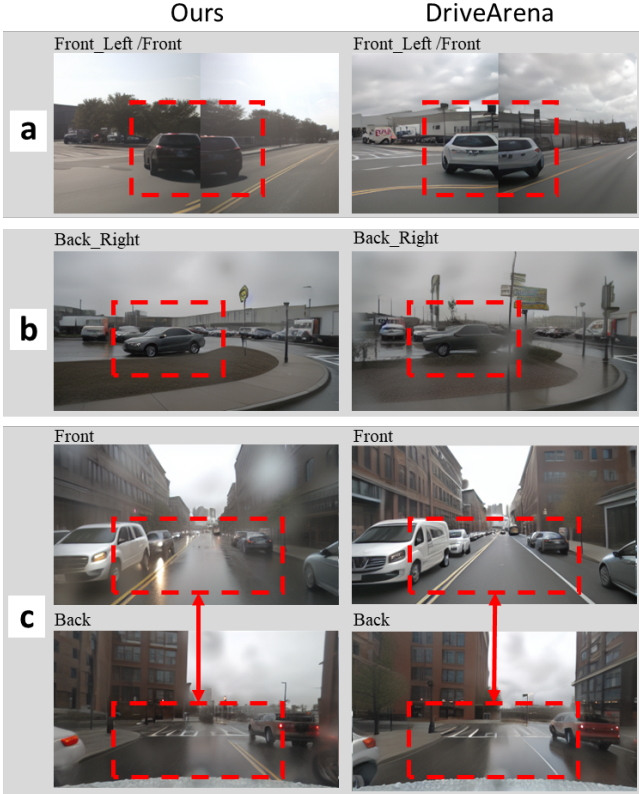


Fig. 4: **Comparison of generated image quality.** We generate three sets of example images: a, b, and c. In sub-figures a and b, the elements within the red boxes clearly show that our generator generates higher-quality images. In sub-figure c, it can be observed that both the front and back views are consistently rainy, while the baseline shows noticeable differences.

images. UniAD, as the evaluator, is performed on these generated images and computes the perception-related metrics, including 3d object detection(3DOD), bird’s-eye view(BEV) segmentation. The experimental results are shown in TABLE II. The results indicate that the gap between the generated image by our model and the original nuScenes is minimal in most perception metrics. This also shows that our generator is highly controllable and can generate images strictly according to conditions. Meanwhile, we present some generated results, as shown in Fig. 4. From the three sets of different generated images, it can be seen that our generation quality is obviously higher. In sub-figure c of Fig. 4, our generator can generate road conditions with rainy weather for both the front and back views, while the baseline exhibits noticeable differences between the front and back views.

C. Adversarial Closed-loop Experiments

We conduct tests on two representative end-to-end models, UniAD and VAD, using the official code and pre-trained weights. We experiment with various adversarial scenarios, including cut-ins, sudden braking of leading vehicles, intersection games, and rapid merges etc. The closed-loop

Data Source	3DOD↑		BEV Segmentation mIoU (%)↑			
	mAP	NDS	Lanes	Driveable	Divider	Crossing
Original	37.93	43.67	31.31	69.15	25.94	14.37
MagicDrive [20]	14.54	27.00	23.53	54.63	18.93	6.48
DriveArena [22]	16.36	28.83	28.37	62.54	22.69	10.84
Ours	18.46	29.93	28.52	63.07	23.05	10.75

TABLE II: **Comparison of fidelity in generating important traffic information.** Generated images are input into UniAD to compare perception results. Original represents using the original real image as input. The **bolded result** denotes the smallest gap between the perception results of the generated images and the original real images.

ablation results with and without adversarial traffic are summarized in TABLE III. Initially, in a traffic environment without adversarial surrounding vehicles, both UniAD and VAD achieved both SC and RC above 0.8, with good performance across all metrics. However, after introducing adversarial surrounding vehicles, the comprehensive scores PDMS and DS dropped significantly by 30 %–50 %, and the completion rates SC and RC also decrease significantly. These results indicate that adversarial surrounding vehicles create numerous corner cases to challenge the end-to-end models. This notable performance decline highlights the weakness of current end-to-end driving models when facing adversarial traffic participants. Although UniAD and VAD can perform well under steady driving conditions, they still lack the capability to handle rare and safety-critical interactions. This also exposes the limitations of purely imitation learning in out-of-distribution scenarios.

To further demonstrate the impact of adversarial vehicles, we present a typical case study. Fig. 5 shows the evaluation scene, including the traffic flow, the generated images, and the output of the tested model. From the results, it can be observed that without adversarial vehicles, both UniAD and VAD pass successfully. However, when adversarial surrounding vehicles are introduced, UniAD fails to effectively avoid a collision when faced with an aggressive cut-in from the vehicle ahead, and VAD fails to make an avoidance maneuver and causes a collision in the intersection game scenario. It can be observed that the generated images have high fidelity, almost indistinguishable from real traffic scenes. The adversarial vehicles maintain consistency in both temporal and perspectival aspects, and their direction and positioning are generated accurately. Therefore, it can be concluded that the failure of the ego is due to the safety-critical corner case created by the adversarial interaction of the surrounding vehicles rather than image quality. This example demonstrates that our adversarial platform can effectively expose the limitations and potential problems of end-to-end models while maintaining a high level of scenario realism.

IV. CONCLUSIONS

This paper introduces an innovative real-world adversarial closed-loop evaluating platform that integrates a Real-World

Tesed Model	Traffic Condition	NC↑	DAC↑	TTC↑	C↑	EP↑	PDMS↑	RC↑	DS↑	SC↑
UniAD	w/o adv	0.892	0.976	0.851	0.798	0.752	0.721	0.905	0.683	0.867
	w/ adv	0.550	0.978	0.661	0.747	0.742	0.430	-0.291	0.679	-0.226
VAD	w/o adv	0.854	0.929	0.835	0.999	0.737	0.674	0.848	0.615	0.806
	w/ adv	0.574	0.941	0.733	1.000	0.711	0.446	-0.228	0.648	-0.200

TABLE III: **Ablation results of adversarial closed-loop evaluation.** The metrics with a gray background are comprehensive closed-loop scores and completion rates, and the numbers in small font represent the scores or completion rates reduction in adversarial traffic flow compared to steady traffic flow. The adv in the table represents adversarial traffic.

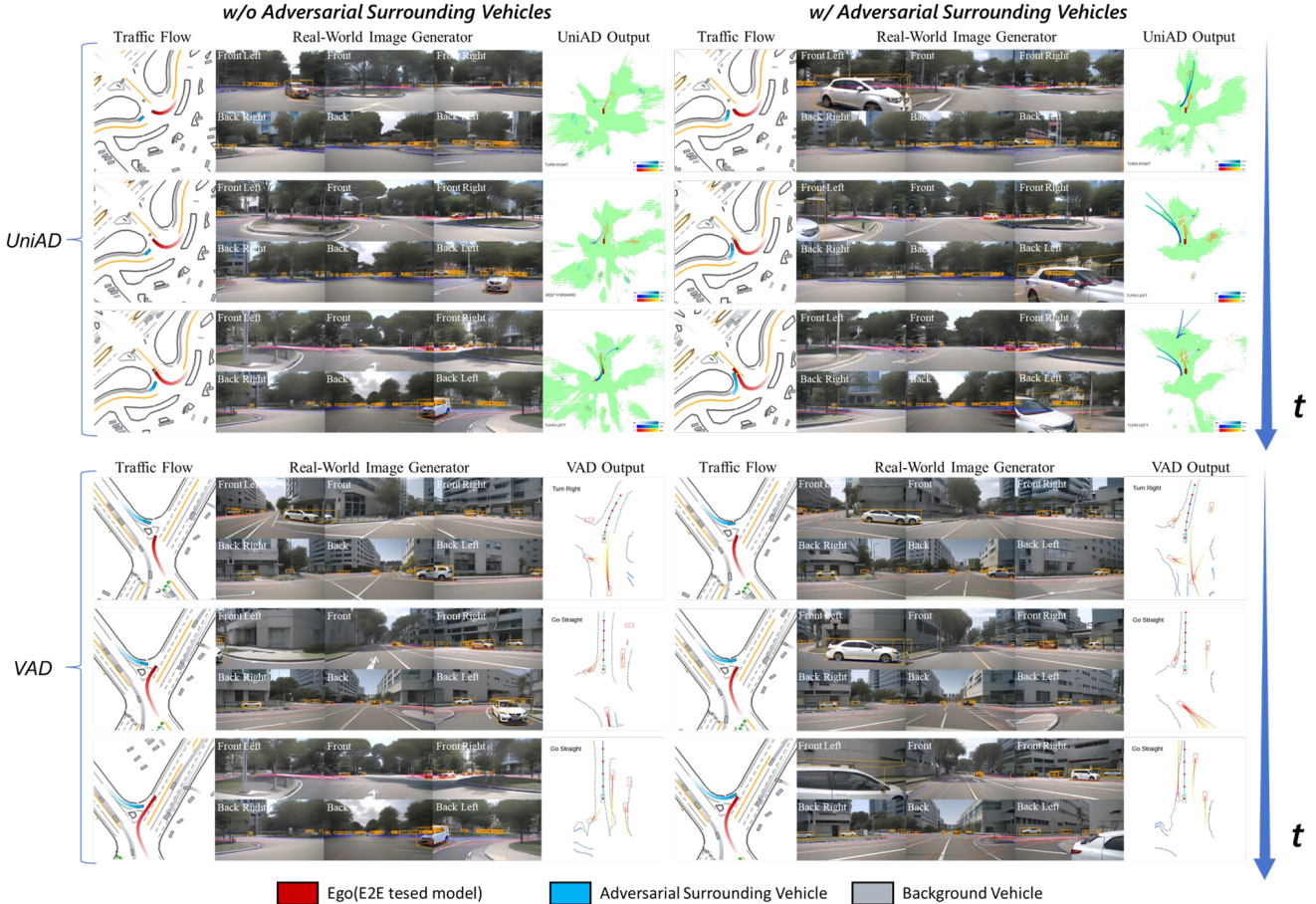


Fig. 5: **A typical case in adversarial closed-loop evaluating.** The top and bottom sections show the performance of UniAD and VAD, and we capture three key frames from the interaction. In each cell, the left side displays the ground truth traffic flow extracted from MetaDrive. The center shows the generated image from the Real-World Image Generator. The right side displays the output of the tested end-to-end model.

Image Generator and Adversarial Traffic Flow to perform adversarial interaction testing on E2E Tested Models trained on the real-world dataset. The flow matching method in the generator ensures the quality of generated real-world images under low denoising steps, significantly improving the efficiency of real-world closed-loop evaluation. Adversarial traffic flow is explored through a two-episode design to select the most adversarial surrounding vehicles' trajectories for different end-to-end tested models. Experimental results show that the realism metrics of the images generated by our platform are better than those of the baseline, and the

generator has strong controllability over key traffic elements in the generated images. By the fast, high-quality image generator and adversarial traffic policy, we can create adversarial scenarios that tested models fail to cover. Although representative end-to-end models like UniAD and VAD perform well under steady traffic conditions, they exhibit potential issues in adversarial closed-loop scenarios, with significant drops in scores and completion rate. In conclusion, the proposed platform provides a valuable tool for evaluating end-to-end autonomous driving in corner cases.

REFERENCES

[1] P. S. Chib and P. Singh, “Recent advancements in end-to-end autonomous driving using deep learning: A survey,” *IEEE Transactions on Intelligent Vehicles*, vol. 9, no. 1, pp. 103–118, 2023.

[2] L. Chen, P. Wu, K. Chitta, B. Jaeger, A. Geiger, and H. Li, “End-to-end autonomous driving: Challenges and frontiers,” *IEEE Transactions on Pattern Analysis and Machine Intelligence*, 2024.

[3] Y. Hu, J. Yang, L. Chen, K. Li, C. Sima, X. Zhu, S. Chai, S. Du, T. Lin, W. Wang *et al.*, “Planning-oriented autonomous driving,” in *Proceedings of the IEEE/CVF conference on computer vision and pattern recognition*, 2023, pp. 17 853–17 862.

[4] B. Jiang, S. Chen, Q. Xu, B. Liao, J. Chen, H. Zhou, Q. Zhang, W. Liu, C. Huang, and X. Wang, “Vad: Vectorized scene representation for efficient autonomous driving,” in *Proceedings of the IEEE/CVF International Conference on Computer Vision*, 2023, pp. 8340–8350.

[5] H. Wang, P. Cai, R. Fan, Y. Sun, and M. Liu, “End-to-end interactive prediction and planning with optical flow distillation for autonomous driving,” in *Proceedings of the IEEE/CVF Conference on Computer Vision and Pattern Recognition*, 2021, pp. 2229–2238.

[6] N. Hanselmann, K. Renz, K. Chitta, A. Bhattacharyya, and A. Geiger, “King: Generating safety-critical driving scenarios for robust imitation via kinematics gradients,” in *European Conference on Computer Vision*. Springer, 2022, pp. 335–352.

[7] D. Rempe, J. Philion, L. J. Guibas, S. Fidler, and O. Litany, “Generating useful accident-prone driving scenarios via a learned traffic prior,” in *Proceedings of the IEEE/CVF Conference on Computer Vision and Pattern Recognition*, 2022, pp. 17 305–17 315.

[8] J. Wang, A. Pun, J. Tu, S. Manivasagam, A. Sadat, S. Casas, M. Ren, and R. Urtasun, “Advsim: Generating safety-critical scenarios for self-driving vehicles,” in *Proceedings of the IEEE/CVF Conference on Computer Vision and Pattern Recognition*, 2021, pp. 9909–9918.

[9] W. Ding, B. Chen, B. Li, K. J. Eun, and D. Zhao, “Multimodal safety-critical scenarios generation for decision-making algorithms evaluation,” *IEEE Robotics and Automation Letters*, vol. 6, no. 2, pp. 1551–1558, 2021.

[10] B. Chen, X. Chen, Q. Wu, and L. Li, “Adversarial evaluation of autonomous vehicles in lane-change scenarios,” *IEEE transactions on intelligent transportation systems*, vol. 23, no. 8, pp. 10 333–10 342, 2021.

[11] A. Dosovitskiy, G. Ros, F. Codevilla, A. Lopez, and V. Koltun, “Carla: An open urban driving simulator,” in *Conference on robot learning*. PMLR, 2017, pp. 1–16.

[12] Q. Li, Z. Peng, L. Feng, Q. Zhang, Z. Xue, and B. Zhou, “Metadrive: Composing diverse driving scenarios for generalizable reinforcement learning,” *IEEE transactions on pattern analysis and machine intelligence*, vol. 45, no. 3, pp. 3461–3475, 2022.

[13] D. Krajzewicz, J. Erdmann, M. Behrisch, L. Bieker *et al.*, “Recent development and applications of sumo-simulation of urban mobility,” *International journal on advances in systems and measurements*, vol. 5, no. 3&4, pp. 128–138, 2012.

[14] A. Hu, L. Russell, H. Yeo, Z. Murez, G. Fedoseev, A. Kendall, J. Shotton, and G. Corrado, “Gaia-1: A generative world model for autonomous driving,” *arXiv preprint arXiv:2309.17080*, 2023.

[15] Y. Wang, J. He, L. Fan, H. Li, Y. Chen, and Z. Zhang, “Driving into the future: Multiview visual forecasting and planning with world model for autonomous driving,” in *Proceedings of the IEEE/CVF Conference on Computer Vision and Pattern Recognition*, 2024, pp. 14 749–14 759.

[16] X. Wang, Z. Zhu, G. Huang, X. Chen, J. Zhu, and J. Lu, “Drive-dreamer: Towards real-world-drive world models for autonomous driving,” in *European conference on computer vision*. Springer, 2024, pp. 55–72.

[17] A. Swerdlow, R. Xu, and B. Zhou, “Street-view image generation from a bird’s-eye view layout,” *IEEE Robotics and Automation Letters*, vol. 9, no. 4, pp. 3578–3585, 2024.

[18] K. Yang, E. Ma, J. Peng, Q. Guo, D. Lin, and K. Yu, “Bevcontrol: Accurately controlling street-view elements with multi-perspective consistency via bev sketch layout,” *arXiv preprint arXiv:2308.01661*, 2023.

[19] Y. Wen, Y. Zhao, Y. Liu, F. Jia, Y. Wang, C. Luo, C. Zhang, T. Wang, X. Sun, and X. Zhang, “Panacea: Panoramic and controllable video generation for autonomous driving,” in *Proceedings of the IEEE/CVF Conference on Computer Vision and Pattern Recognition*, 2024, pp. 6902–6912.

[20] R. Gao, K. Chen, E. Xie, L. Hong, Z. Li, D.-Y. Yeung, and Q. Xu, “Magicdrive: Street view generation with diverse 3d geometry control,” *arXiv preprint arXiv:2310.02601*, 2023.

[21] Z. Xu, B. Li, H.-a. Gao, M. Gao, Y. Chen, M. Liu, C. Yan, H. Zhao, S. Feng, and H. Zhao, “Challenger: Affordable adversarial driving video generation,” *arXiv preprint arXiv:2505.15880*, 2025.

[22] X. Yang, L. Wen, Y. Ma, J. Mei, X. Li, T. Wei, W. Lei, D. Fu, P. Cai, M. Dou *et al.*, “Drivearena: A closed-loop generative simulation platform for autonomous driving,” *arXiv preprint arXiv:2408.00415*, 2024.

[23] S. Kuutti, S. Fallah, and R. Bowden, “Training adversarial agents to exploit weaknesses in deep control policies,” in *2020 IEEE International Conference on Robotics and Automation (ICRA)*. IEEE, 2020, pp. 108–114.

[24] M. Koren, A. Nassar, and M. J. Kochenderfer, “Finding failures in high-fidelity simulation using adaptive stress testing and the backward algorithm,” in *2021 IEEE/RSJ International Conference on Intelligent Robots and Systems (IROS)*. IEEE, 2021, pp. 5944–5949.

[25] Z. Wang, X. Li, D. Wei, L. Wang, and Y. Huang, “Efficient generation of safety-critical scenarios combining dynamic and static scenario parameters,” *IEEE Transactions on Intelligent Vehicles*, 2024.

[26] W. Ding, B. Chen, M. Xu, and D. Zhao, “Learning to collide: An adaptive safety-critical scenarios generating method,” in *2020 IEEE/RSJ International Conference on Intelligent Robots and Systems (IROS)*. IEEE, 2020, pp. 2243–2250.

[27] L. Zhang, Z. Peng, Q. Li, and B. Zhou, “Cat: Closed-loop adversarial training for safe end-to-end driving,” in *Conference on Robot Learning*. PMLR, 2023, pp. 2357–2372.

[28] X. Zhang, Z. Zhou, Z. Wang, Y. Ji, Y. Huang, and H. Chen, “Co-mtp: A cooperative trajectory prediction framework with multi-temporal fusion for autonomous driving,” in *2025 IEEE International Conference on Robotics and Automation (ICRA)*. IEEE, 2025, pp. 801–807.

[29] X. Liu, C. Gong, and Q. Liu, “Flow straight and fast: Learning to generate and transfer data with rectified flow,” *arXiv preprint arXiv:2209.03003*, 2022.

[30] Z. Zhou, D. Chen, C. Wang, and C. Chen, “Fast ode-based sampling for diffusion models in around 5 steps,” in *Proceedings of the IEEE/CVF Conference on Computer Vision and Pattern Recognition*, 2024, pp. 7777–7786.

[31] T. Dockhorn, A. Vahdat, and K. Kreis, “Genie: Higher-order denoising diffusion solvers,” *Advances in Neural Information Processing Systems*, vol. 35, pp. 30 150–30 166, 2022.

[32] C. Lu, Y. Zhou, F. Bao, J. Chen, C. Li, and J. Zhu, “Dpm-solver: A fast ode solver for diffusion probabilistic model sampling in around 10 steps,” *Advances in neural information processing systems*, vol. 35, pp. 5775–5787, 2022.

[33] L. Liu, Y. Ren, Z. Lin, and Z. Zhao, “Pseudo numerical methods for diffusion models on manifolds,” *arXiv preprint arXiv:2202.09778*, 2022.

[34] Y. Lipman, R. T. Chen, H. Ben-Hamu, M. Nickel, and M. Le, “Flow matching for generative modeling,” *arXiv preprint arXiv:2210.02747*, 2022.

[35] R. Rombach, A. Blattmann, D. Lorenz, P. Esser, and B. Ommer, “High-resolution image synthesis with latent diffusion models,” in *Proceedings of the IEEE/CVF conference on computer vision and pattern recognition*, 2022, pp. 10 684–10 695.

[36] J. Song, C. Meng, and S. Ermon, “Denoising diffusion implicit models,” *arXiv preprint arXiv:2010.02502*, 2020.

[37] J. Schusterbauer, M. Gui, F. Fundel, and B. Ommer, “Diff2flow: Training flow matching models via diffusion model alignment,” in *Proceedings of the Computer Vision and Pattern Recognition Conference*, 2025, pp. 28 347–28 357.

[38] D. Dauner, M. Hallgarten, T. Li, X. Weng, Z. Huang, Z. Yang, H. Li, I. Gilitschenski, B. Ivanovic, M. Pavone *et al.*, “Navsim: Data-driven non-reactive autonomous vehicle simulation and benchmarking,” *Advances in Neural Information Processing Systems*, vol. 37, pp. 28 706–28 719, 2024.

[39] A. Radford, J. W. Kim, C. Hallacy, A. Ramesh, G. Goh, S. Agarwal, G. Sastry, A. Askell, P. Mishkin, J. Clark *et al.*, “Learning transferable visual models from natural language supervision,” in *International conference on machine learning*. PMLR, 2021, pp. 8748–8763.

[40] S. Ettinger, S. Cheng, B. Caine, C. Liu, H. Zhao, S. Pradhan, Y. Chai, B. Sapp, C. R. Qi, Y. Zhou *et al.*, “Large scale interactive motion forecasting for autonomous driving: The waymo open motion dataset,”

in *Proceedings of the IEEE/CVF international conference on computer vision*, 2021, pp. 9710–9719.

[41] J. Gu, C. Sun, and H. Zhao, “Densentnt: End-to-end trajectory prediction from dense goal sets,” in *Proceedings of the IEEE/CVF international conference on computer vision*, 2021, pp. 15 303–15 312.